Aerosol-Assisted Chemical Vapor Deposition of Lubricating MoS_2 Films. Ferrous Substrates and Titanium Film Doping

Matthew N. McCain,[†] Bo He,[‡] Javad Sanati,[‡] Q. Jane Wang,[*,‡] and Tobin J. Marks[*,†]

Department of Chemistry, Materials Research Center, and Department of Mechanical Engineering, Northwestern University, 2145 Sheridan Road, Evanston, Illinois 60208-3113

Received September 18, 2007. Revised Manuscript Received May 13, 2008

MoS_2 thin films have been deposited onto 52100 steel substrates by aerosol-assisted chemical vapor deposition using the metal-organic precursor tetrakis(diethyl-dithiocarbamato)molybdenum(IV) (**1**). Analysis of the films indicates growth of an initial, highly crystalline FeS layer exhibiting preferred orientation parallel to the substrate, followed by growth of MoS_2 nanoparticles. Friction coefficients for MoS_2-coated steel specimens reach 0.10 when tested at 100 °C in air. Tetrakis(*tert*-butylthiolato)titanium(IV) (**2**), dissolved with complex **1** in THF solutions, yields nanoparticle films of variable TiO_2 content as a result of solvent decomposition on MoS_2 and subsequent in situ reaction with the titanium precursor.

Introduction

MoS_2 has been used for decades as a solid lubricant material, with particular application in high-vacuum environments,[1] and finds wide application in slow rolling or sliding contacts, releases, and precision-bearing applications. In comparison to fluid lubricants, MoS_2 is preferred in vacuum because of low outgassing pressure and lack of migration. MoS_2, having a modulated crystal structure consisting of sandwiched S−Mo−S layers,[2] is thought to function as an intrinsic solid lubricant. Weak van der Waals' forces between the MoS_2 layers allow lubrication via mutual sliding between the layers.[3] Other applications of this material include high-density batteries because of its appreciable electrical conductivity and ability to reversibly intercalate Li.[4] The optical and electronic properties of MoS_2 also make it a candidate for efficient solar energy cells,[5] and MoS_2 has been successfully used in materials for dehydrosulfurization/hydrogenation catalysis.[6]

As lubricants, MoS_2 films exhibit low friction coefficients and long lifetimes in dry air and/or inert or vacuum environments.[1] To date, MoS_2 thin films have been grown by a variety of methods, predominately via radio frequency sputtering,[7] but also by pulsed laser deposition,[8] chemical vapor transport,[9] and chemical vapor deposition.[10] Chemical vapor deposition (CVD) is a well-developed technique for growing thin films of a wide variety of materials.[11] Compared to r. f. sputtering, CVD offers the attractions of conformal surface coverage at closer to ambient conditions, simpler apparatus, and the possibility of creating metastable phases. However, a major limitation of this method is the requirement

* Corresponding author. E-mail: t-marks@northwestern.edu..
† Department of Chemistry, Materials Research Center, Northwestern University.
‡ Department of Mechanical Engineering, Northwestern University.

(1) (a) Hilton, M. R.; Bauer, R.; Didziulis, S. V.; Dugger, M. T.; Keem, J. M.; Scholhamer, J. *Surf. Coat. Technol.* **1992**, *53*, 13–23. (b) *Fundamental in Friction: Macroscopic and Microscopic Processes*; Singer, I. L.,Pollock, H. M., Eds.; Kluwer: Dordrecht, The Netherlands, 1992; p 237. (c) Roberts, E. W. *Tribol. Int.* **1990**, *23*, 95–104. (d) Spalvins, T. *J. Vac. Sci.Technol., A* **1987**, *5*, 212–19.

(2) Dickinson, R. G.; Pauling, L. *J. Am. Chem. Soc.* **1923**, *45*, 1466–1471.

(3) (a) Fleischauer, P. D. *Thin Solid Films* **1987**, *154*, 309–322. (b) Holinski, R.; Gansheimer, J. *Wear* **1972**, *19*, 329–342.

(4) (a) Pramanik, P.; Bhattacharya, S. *Mater. Res. Bull.* **1990**, *25*, 15–23. (b) Simon, R. A.; Ricco, A. J.; Harrison, J.; Wrighton, M. S. *J. Phys. Chem.* **1983**, *87*, 4446–4453.

(5) (a) Shin, H.; Doerr, J.; Deshpandey, C. V.; Dunn, B.; Bunshah, R. F. *Surf. Coat. Technol.* **1989**, *39* (40), 683–690. (b) Auburn, J. J.; Barberio, Y. L.; Hanson, K. J.; Schleich, D. M.; Martin, M. *J. Electrochem. Soc.* **1987**, *134*, 580–586.

(6) (a) Boone, W. P.; Ekerdt, J. G. *J. Catal.* **2000**, *193*, 96–102. (b) Scholz, G. A.; Morrison, S. R. *Can. J. Chem.* **1989**, *86*, 2–866. (c) Miremadi, B. K.; Morrison, S. R. *J. Catal.* **1988**, *112*, 418–426.

(7) (a) Koguma, K.; Ikeda, M.; Ota, N.; Matsuda, K.; Kaneta, M. *J. Vac. Sci. Technol., A* **2007**, *25*, 324–329. (b) Jakovidis, G.; Jamieson, I. M.; Singh, A. *Surf. Rev. Lett.* **2003**, *10*, 443–448. (c) Suzuki, M. *Lubr. Eng.* **2001**, *57*, 23–29. (d) Moser, J.; Levy, F.; Bussy, F. *J. Vac. Sci. Technol., A* **1994**, *12*, 494–500. (e) Cong, Q.; Yu, D.; Wang, J.; Ou, Y. J. *Thin Solid Films* **1992**, *209*, 1–8. (f) Lince, J. R. *J. Mater. Res.* **1990**, *218*, 895. (g) Donley, M. S.; Mcdevltt, N. T.; Haas, T. W.; Murray, P. T.; Grant, J. T. *Thin Solid Films* **1989**, *168*, 335–344. (h) Bertrand, P. A. *J. Mater. Res.* **1989**, *4*, 180–4.

(8) (a) Donley, M. S.; McDevitt, N. T.; Haas, T. W.; Murray, P. T.; Grant, J. T. *Thin Solid Films* **1989**, *168*, 335–44. (b) Donley, M. S.; Murray, P. T.; Barber, S. A.; Haas, T. W. *Surf. Coat. Technol.* **1988**, *36*, 329–40.

(9) (a) Dave, M.; Vaidya, R.; Patel, S. G.; Jani, A. R. *Bull. Mater. Sci.* **2004**, *27*, 213–216. (b) Tiong; K, K.; Huang, Y. S.; Ho, C. H. *J. Alloys Compd.* **2001**, *31*, 7–318, 208−212.

(10) (a) Etzkorn, J.; Therese, H. A.; Rocker, F.; Zink, N.; Kolb, U.; Tremel, W. *Adv. Mater.* **2005**, *17*, 2372–2375. (b) Cheon, J.; Gozum, J. E.; Girolami, G. S. *Chem. Mater.* **1997**, *9*, 1847–1853.

(11) (a) Rodriguez-Castro, J.; Dale, P.; Mahon, M. F.; Molloy, K. C.; Peter, L. M. *Chem. Mater.* **2007**, *19*, 3219–3226. (b) Shulz, D. L.; MarksT. J. In *CVD of Non-Metals*; Rees, W., Ed.; VCH: New York, 1996; 39−150. (c) McCain, M. N.; Metz, A. W.; Yang, Y.; Stern, C. L.; Marks, T. J. *Chem. Vap. Deposition* **2005**, *11*, 291–294. (d) Metz, A. W.; Ireland, J. R.; Zheng, J.-G.; Lobo, R. P. S. M.; Yang, Y.; Ni, J.; Stern, C. L.; Dravid, V. P.; Bontemps, N.; Kannewurf, C. R.; Poeppelmeier, K. R.; Marks, T. J. *J. Am. Chem. Soc.* **2004**, *126*, 8477–8492. (e) Choy, K. L. *Prog. Mat. Sci.* **2003**, *48*, 57–170. (f) Chi, K.-M.; Lu, Y.-H. *Chem. Vap. Deposition* **2001**, *7*, 117–120. (g) Belot, J. A.; Wang, A.; McNeely, R. J.; Liable-Sands, L.; Rheingold, A. L.; Marks, T. J. *Chem. Vap. Deposition* **1999**, *5*, 65–69. (h) Belot, J. A.; Neumayer, D. A.; Reedy, C. J.; Studebaker, D. B.; Hinds, B. J.; Stern, C. L.; Marks, T. J. *Chem. Mater.* **1997**, *9*, 1638. (i) Schulz, D. L.; Marks, T. J. *Adv. Mater.* **1994**, *6*, 719.

10.1021/cm7026674 CCC: $40.75 © 2008 American Chemical Society
Published on Web 08/06/2008

of highly volatile metal-organic precursors. In comparison, aerosol-assisted (AA) CVD has been recently developed to utilize metal precursors with lower volatilities, without sacrificing film quality.[12] Recently, researchers used tetrakis(diethyldithiocarbamato)molybdenum(IV) to grow MoS_2 thin films by AACVD on glass substrates.[13] These films grow with preferential orientation of the MoS_2 layers parallel to the glass substrate. Nevertheless, further studies will be required to determine if MoS_2 films deposited by AACVD on realistic substrates such as steel will exhibit the low friction coefficients required for efficient tribological coatings.[14]

At higher temperatures, in the presence of water vapor, the tribological efficiency of MoS_2 is significantly compromised.[15] Oxidation to MoO_3 and H_2SO_4 appreciably increases the friction coefficient. However, it has been shown that MoS_2 film resistance to oxidation in atmospheric environments increases when films are deposited with the addition of a second metal in a multilayer or composite structure.[16] Codeposition of various metals with MoS_2 has been extensively studied, and MoS_2 composite coatings with Ti incorporation were recently reported to exhibit an order of magnitude enhancement in wear endurance in moist air, compared to pure MoS_2 films.[17] To the best of our knowledge, all of this work was carried out using physical vapor deposition techniques, consisting primarily of r. f. sputtering of MoS_2 and Ti sources, or by sulfurizing Mo−Ti alloys with sulfur-containing gases (e.g., H_2S).[18]

Studies of MoS_2 composite coating growth with Ti incorporation have not been reported using aerosol-assisted CVD. However, tetrakis(*tert*-butylthiolato)titanium(IV) has been used to grow TiS_2 films by AACVD,[19] and titanium disulfide is also of interest as a high-temperature solid lubricant[20] and an active cathode material for high-density batteries.[21] Similar to MoS_2, the crystal structure of TiS_2 consists of parallel layers bound by weak van der Waals' forces. In this contribution, we report the growth and friction characterization of AACVD-derived MoS_2 films on 52100 steel substrates using $Mo(S_2CNEt_2)_4$ as the precursor. We also explore the possibility of incorporating Ti into the MoS_2 structure using the molecular precursor $Ti(S^tBu)_4$.

Experimental Section

Materials and Methods. All manipulations of air-sensitive materials were carried out with rigorous exclusion of oxygen and moisture in flame- or oven-dried Schlenk-type glassware on a dual-manifold Schlenk line, or in a nitrogen-filled Vacuum Atmospheres or MBraun glovebox with a high-capacity recirculator (<2 ppm O_2). Tetrakis(diethyldithiocarbamato)molybdenum(IV)[22] (**1**) and tetrakis(*tert*-butylthiolato)titanium(IV)[23] (**2**) were synthesized and purified according to literature methods. The purity of these compounds was confirmed by elemental analysis, electron spray ionization mass spectroscopy, and NMR spectroscopy. Thermogravimetric analysis (TGA) was performed on a TA Instruments Q50 thermogravimetric analyzer at a ramp rate of 2.5 °C min^{-1} and under a N_2 flow rate of 90 mL min^{-1} at atmospheric pressure.

Film Growth and Characterization. Thin films were grown in a horizontal cold-wall quartz reactor with liquid aerosol injection at atmospheric pressure and solvent trap and bubbler for exhaust gas. Precursor solutions were nebulized with a TSI 3076 collision-type nebulizer and were deposited on substrates downstream in the reactor. Carrier gas (Ar) flow rates were controlled at 1.6 L/min by a mass flow controller. Substrates were cleaned with acetone and placed on the graphite susceptor in the reactor. They were heated by an infrared lamp. The reactor was evacuated and backfilled with Ar three times prior to film growth experiments, and the precursor reservoir was charged with freshly prepared precursor solutions in tetrahydrofuran ($[Mo(S_2CNEt_2)_4] = 0.015$ M, $[Ti(S^tBu)_4] = 0$ - 0.0075 M) via cannula filtration (Whatman GF/B glass fiber filters). The optimum susceptor temperature for high growth rates and crystallinity of the MoS_2 films was found, after some experimentation, to be 400 °C. For the simultaneous growth of MoS_2 and TiO_2 films, the optimum susceptor temperature was determined to be 350 °C. Film thicknesses were measured with a Tencor P-10 profilometer. Film compositions were assayed using inductively coupled plasma optical emission spectroscopy (ICP/OES) with a Varian Vista MPX ICP-OES spectrometer after films were dissolved in nitric acid. X-ray photoelectron spectroscopy (XPS) of films was performed on an Omicron ESCAPROBE system using Al Kα radiation. Glancing X-ray diffraction (GXRD) (angle of incidence $\alpha = 0.3°$) $\theta-2\theta$ scans were performed on a computer-interfaced Rigaku ATX-G diffractometer. Film microstructure and morphologies were assessed with an FEI Quanta 600sFEG scanning electron microscope (SEM) and JEOL JEM-2100F FAST transmission electron microscope (TEM). Friction measurements were performed on a Micro Materials Nanotest tribometer using a 25 mm Rockwell tip, a normal load of 10 mN, and a scan rate of 1 μm/s.

(12) (a) Choy, K. L. *Prog. Mater. Chem.* **2003**, *48*, 57–170. (b) Schäfer, P.; Waser, R. *Adv. Mater. Opt. Electron.* **2000**, *10*, 169–175. (c) KodasT. T.; Hampden-Smith, M. J. *Aerosol Processing of Materials*; Wiley: New York, 1999. (d) Hubert-Pfalzgraf, L. G.; Guillon, H. *Appl. Organomet. Chem.* **1998**, *12*, 221–236. (e) Roger, C.; Corbitt, T.; Xu, C.; Zeng, D.; Powell, Q.; Chandler, C. D.; Nyman, M.; Hampden-Smith, M. J.; Kodas, T. T. *Nanostruct. Mater.* **1994**, *4*, 529–35. (f) *The Chemistry of Metal CVD* Kodas, T., Hampden-Smith, M., Eds.; VCH: Weinheim, Germany, 1994.

(13) Adeogun, A.; Afzaal, M.; O'Brien, P. *Chem. Vap. Deposition* **2006**, *12*, 597–599.

(14) Fleischauer, P. D.; Lince, J. R. *Tribol. Int.* **2000**, *32*, 627–636.

(15) (a) Suzuki, M. *Lubr. Eng.* **2001**, *57*, 23–29. (b) Wahl, K. J.; Belin, M.; Singer, I. L. *Wear* **1998**, *214*, 212–220. (c) Singer, I. L.; Fayeulle, S.; Ehni, P. D. *Wear* **1996**, *195*, 7–20.

(16) (a) Savan, A.; Pfluger, E.; Voumard, P.; Schroer, A.; Simmonds, M. *Lubr. Sci.* **2000**, *12*, 185–203. (b) Stupp, B. C. *Thin Solid Films* **1981**, *84*, 257–66.

(17) (a) Renevier, N. M.; Fox, V. C.; Teer, D. G.; Hampshire, J. *Surf. Coat. Technol.* **2000**, *127*, 24–37. (b) Fox, V. C.; Renevier, N.; Teer, D. G.; Hampshire, J.; Rigato, V. *Surf. Coat. Technol.* **1999**, *11*, 6–119, 492−497.

(18) (a) Picas, J. A.; Forn, A.; Baile, M.; Martin, E. *Surf. Eng.* **2006**, *22*, 314–319. (b) Arslan, E.; Buelbuel, F.; Efeoglu, I. *Tribol. Trans.* **2004**, *47*, 218–226. (c) Renevier, N. M.; Hamphire, J.; Fox, V. C.; Witts, J.; Allen, T.; Teer, D. G. *Surf. Coat. Technol.* **2001**, *14*, 2–144, 67−77. (d) Bae, Y. W.; Lee, W. Y.; Besmann, T. M.; Yust, C. S.; Blau, P. J. *Mater. Sci. Eng., A* **1996**, *A209*, 372–376.

(19) Carmalt, C. J.; Dinnage, C. W.; Parkin, I. P.; White, A. J. P.; Williams, D. J. *J. Chem. Soc., Dalton Trans.* **2001**, *255*, 4–2558.

(20) (a) Subramonian, B.; Kato, K.; Adachi, K.; Basu, B. *Tribol. Lett.* **2005**, *20*, 263–272. (b) Margolin, A.; Popovitz-Biro, R.; Albu-Yaron, A.; Rapoport, L.; Tenne, R. *Chem. Phys. Lett.* **2005**, *411*, 162–166. (c) Bill, R. C. *Wear* **1985**, *106*, 283–301.

(21) (a) Frazer, E. J.; Phang, S. *J. Power Sources* **1981**, *6*, 307–17.

(22) Decoster, M.; Conan, F.; Guerchais, J. E.; Mest, Y. L.; Jeffery, J. C.; Faulques, E.; Leblanc, A.; Molinie, P. *Polyhedron* **1995**, *14*, 1741–1750.

(23) Cheon, J.; Gozum, J. E.; Girolami, G. S. *Chem. Mater.* **1997**, *9*, 1847–1853.

(24) Ouyang, T.; Loh, K. P.; Zhang, H.; Vittal, J. J.; Vetrichelvan, M.; Chen, W.; Gao, X.; Wee, A. T. S. *J. Phys. Chem. B* **2004**, *108*, 17537–17545.

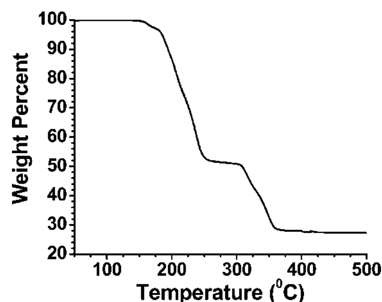

Figure 1. Atmospheric pressure thermogravimetric analysis (TGA) of the volatility characteristics of $Mo(S_2CNEt_2)_4$ (**1**). The weight loss data were recorded at a ramp rate of 2.5 °C/min and at 50 mL/min N_2 flow rate at 1.0 atm pressure.

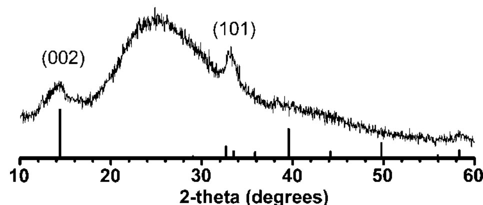

Figure 2. X-ray diffraction (XRD) $\theta-2\theta$ scan of MoS_2 film **A** grown on glass by AACVD using precursor **1**. Peaks are labeled with the corresponding (*hkl*) reflections from the hexagonal phase of MoS_2 (PDF 37−1492). Underneath is the peak positions and relative intensities for the powder pattern for MoS_2 (PDF 37−1492).

Results

AACVD of MoS_2 Thin Films, Film Characterization, and Friction Analysis. The precursor $Mo(S_2CNEt_2)_4$ (**1**) was prepared and purified according to a literature procedure,[22] and purity was assessed accordingly via elemental analysis and electron spray ionization mass spectrometry. In evaluating precursor performance for AACVD growth processes, thermogravimetric analysis (TGA) was performed to assess volatility characteristics. Previously, it had been reported that this compound exhibits a single weight-loss step at 300 °C.[23] Although it was not expressly stated,[23] we assume that this TGA was performed at reduced pressure, as the results differ significantly from ours. Figure 1 shows the atmospheric pressure TGA of precursor **1** under N_2. Decomposition occurs in three steps at ~150, ~180, and ~310 °C. The first and second decomposition steps (−3.8 and −44.1%, respectively) correspond to the calculated weight percent loss of ethylene (−4.0% calcd) and two diethyldithiocarbamate molecules ($2[S_2CNEt_2]$, −42.9% calcd). After the third decomposition step, the residue is a black solid with a residual weight percent of 27.3%. This corresponds to the calculated weight percent loss to produce pure MoS_2 (23.5% calcd), with an additional 3.8% tentatively attributed to decomposed ligand contamination.

MoS_2 Thin Film Growth and Characterization on 52100 Steel. AACVD film growth of MoS_2 films was carried out with 0.015 M solutions of complex **1** in THF simultaneously onto 1737F Corning glass and 52100 steel substrates at 400 °C. Deposited films, 1.5−1.8 μm thick, were black, nonadherent, and relatively amorphous, as judged by the sizable X-ray diffraction (XRD) linewidths (Figure 2). Glancing XRD of the MoS_2 films deposited by AACVD

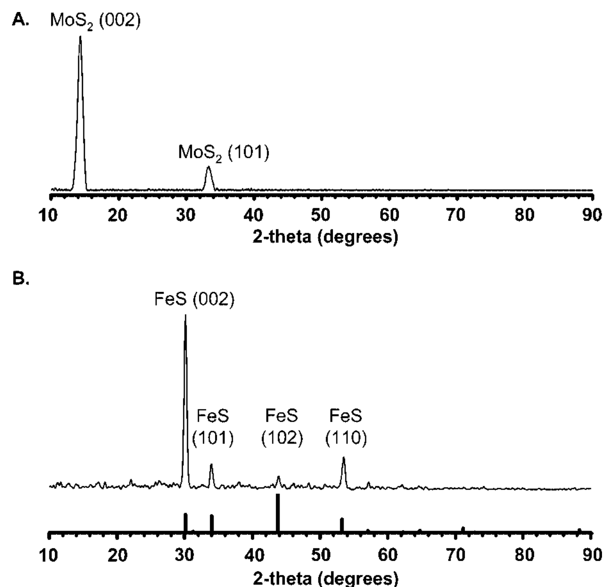

Figure 3. Glancing X-ray diffraction (GXRD) $\theta-2\theta$ scan ($\alpha = 0.30°$) of MoS_2 films grown by AACVD using precursor **1** on (A) Corning 1737F glass and (B) 52100 steel. Peaks are labeled with the corresponding (*hkl*) reflections from hexagonal phase MoS_2 (PDF 37−1492) and FeS (PDF 65−1894). Underneath are the peak positions and relative intensities for the powder pattern of FeS (PDF 65−1894).

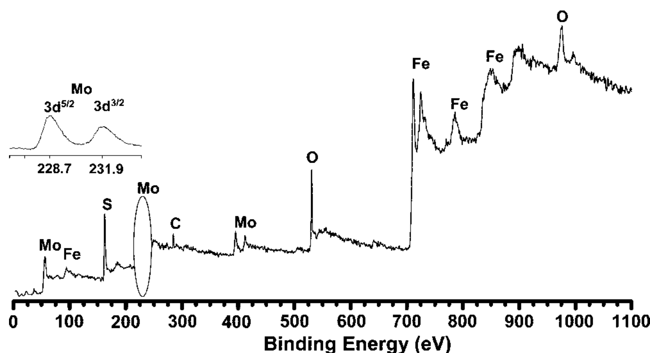

Figure 4. XPS spectrum of MoS_2 film **B** deposited on 52100 steel by AACVD using precursor **1**. Peaks are labeled with their corresponding element. The inset is enlarged portion of the spectrum showing the Mo $3d_{5/2}$ and $3d_{3/2}$ ionizations.

using complex **1** on glass substrates (films **A**) reveals preferred film orientation for the (00 L) planes, with the (101) reflection also visible (Figure 3A). Glancing XRD of MoS_2 films deposited by AACVD using complex **1** on 52100 steel (films **B**) reveals reflections corresponding to the hexagonal phase of FeS (PDF 65−1894, Figure 3B). Preferential orientation is seen as well in the (00*l*) direction. No reflections corresponding to MoS_2 are evident. However, X-ray photoelectron spectroscopy (XPS) does suggest the presence of MoS_2 (Figure 4). Ion sputtering (Ar^+), calibrated at 1.7 nm/min on a silicon wafer, was performed to remove possible surface oxidation. The Mo $3d_{5/2}$ and $3d_{3/2}$ ionization energies (228.7 and 231.9 eV, respectively), as well as the S $2p_{3/2}$ ionization energy (162.2 eV), match well with those reported for MoS_2.[25] Furthermore, the measured Mo/S ratio agrees with the predicted 1:2 stoichiometric ratio by compar-

(25) (a) *Handbook of X-ray Photoelectron Spectroscopy*; Chastain, J., King, R. C., Eds.; Physical Electronics: Eden Prairie, MN, 1995. (b) Stewart, T. B.; Fleischauer, P. D. *Inorg. Chem.* **1982**, *21*, 2426–2431. (c) Grim, S. O.; Matienzo, L. J. *Inorg. Chem.* **1975**, *14*, 1014–1018.

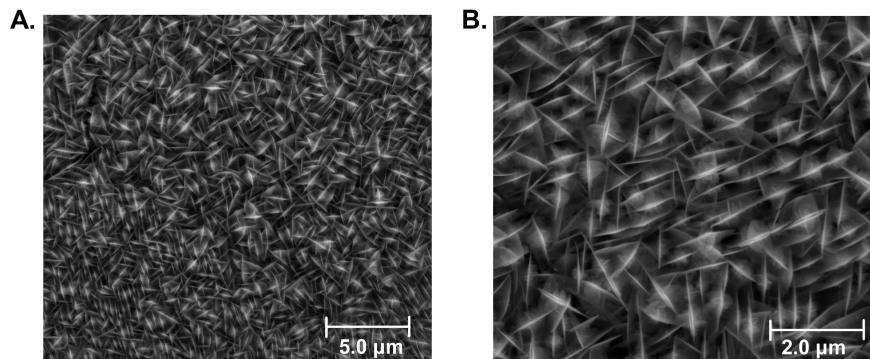

Figure 5. SEM images of MoS_2 film **B** grown on a 52100 steel substrate using precursor **1**.

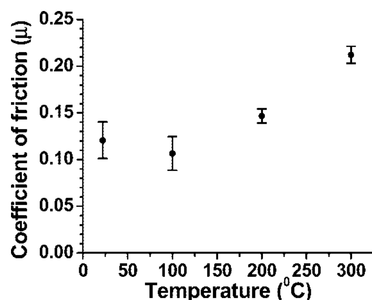

Figure 6. Plot of coefficient of friction (μ) versus temperature in high-temperature scratch tests of an AACVD-derived MoS_2 film **B** grown on 52100 steel using precursor **1**.

ing the peak intensities of the Mo 3d and S 2p ionizations. Other features are evident corresponding to ~1.5% C, as well as to the Fe and O of the substrate. The binding energy of the Fe $2p_{3/2}$ ionization peak (711.2 eV) matches that of iron oxide (709.5 eV for Fe(II)−O[26] 711 eV for Fe(III)−O[26]). Scanning electron microscopy performed on films **B** reveals the films to consist of platelets stacked perpendicular to the surface with dimensions of 0.08 μm × 1 μm (Figure 5). Variable-temperature tribological tests performed on film **B** show that the present MoS_2 films conform to known levels of lubrication for this material (coefficient of friction = 0.12 at room temperature, 0.10 at 100 °C, Figure 6).[14] After conducting high-temperature friction measurements on film **B**, XPS analysis reveals the Mo $3d_{5/2}$ ionization energy has shifted to 232.3 eV, corresponding to Mo^{6+} associated with MoO_3,[28] and the absence of S ionization energies.

Incorporation of Ti into MoS_2 Using $Ti(S^tBu)_4$. Precursor solutions composed of both precursors **1** and **2** dissolved in THF were used to grow films simultaneously onto 1737F amorphous glass and 52100 steel at 350 °C, producing 1.5−1.8 μm thick films as determined by profilometry. The percentage of Ti deposited with the MoS_2 films was varied by changing the molar ratio of complexes **1** and **2** dissolved in the THF precursor solution. Film composition was assayed using ICP/OES mass spectroscopy. Film growth above 370 °C yielded no detectable Ti content. Film growth with toluene solutions of precursors **1** and **2** yielded only MoS_2 films, with negligible Ti content as determined by XPS and ICP/OES. Table 1 lists the concentration used of each precursor and the subsequent percentage of each metal found in films **C**−**F**. GXRD of all the films grown on 52100 steel exhibit reflections assignable to FeS; the $\theta-2\theta$ scans were identical to that shown in Figure 3B. Figure 7 shows the GXRD of films **C**−**F** grown on glass substrates. Film **C**, consisting of 94% Mo and 6% Ti, shows only the MoS_2 phase, with some preferred orientation in the (001) direction. When the level

Table 1. Precursor Solution Concentration of Complexes 1 and 2 in THF Used to Grow Films C−F by AACVD at 350 °C and the Mo,Ti Composition of the Films As Assayed by ICP/OES

precursor solution concentrations (mM)		film composition		film designation
[1]	[2]	% Mo	% Ti	
15	1.5	96	4	C
15	2.9	89	11	D
15	7.2	70	30	E
15	7.5	62	38	F

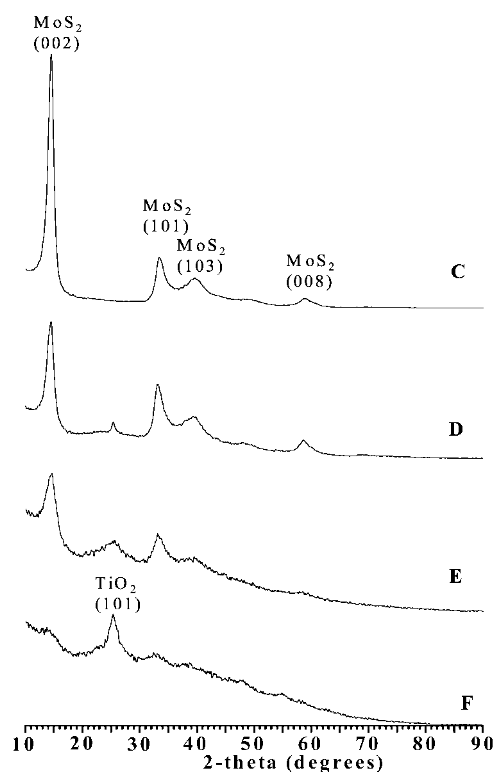

Figure 7. Glancing X-ray diffraction (GXRD) $\theta-2\theta$ scan (ω = 0.30°) of films **C**−**F** grown on 1737F Corning glass by AACVD using precursors **1** and **2**. Peaks are labeled with the corresponding (*hkl*) reflections for hexagonal phase MoS_2 (PDF 37−1492) and tetragonal phase TiO_2 (PDF 71−1166).

(26) McIntyre, N. S.; Zetaruk, D. G. *Anal. Chem.* **1977**, *49*, 1521–1529.
(27) Thomas, J. E.; Jones, C. F.; Skinner, W. M.; Smart, R. St. C. *Geochim. Cosmochim. Act.* **1998**, *62*, 1555–1565.
(28) Barr, T. L. *J. Phys. Chem.* **1976**, *82*, 1801–1810.

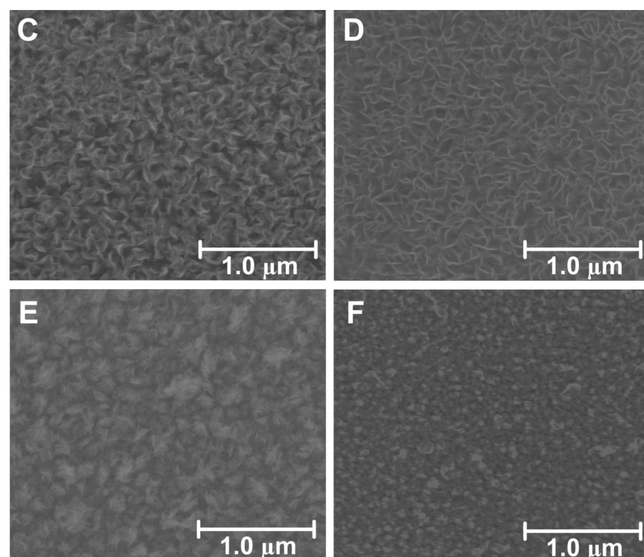

Figure 8. SEM images of MoS_2/TiO_2 films **C**−**F** grown on 1737F Corning glass using precursors **1** and **2**.

of Ti reaches 11% (film **D**), the reflection at $2\theta = 25.3°$ for TiO_2 can be seen. As more Ti is codeposited with the MoS_2, the TiO_2 reflection becomes stronger, and the MoS_2 reflections become weaker.

No visible changes in the morphology are noticeable in the SEM images of films **C**−**F** grown on 52100 steel, compared to film **B**. Figure 8 shows the corresponding SEM images for films **C**−**F** grown on glass substrates. For film **C**, a textured nanoparticle ribbon-like network is observed. This texture is still evident in the GXRD of film **D**, although the visible network in the SEM is diminished. In films **E** and **F**, the observed films consist of small platelets with none of the ribbon-like network observable. Figure 9 shows the XPS scan of film **E**, deposited on 52100 steel, which is representative of all the films. Only the signal intensities vary for films **C**−**F**; peak positions for element ionizations discussed earlier for film **B** are the identical. Judging from the positions of the Mo $3d_{5/2}$ and Ti $2p_{3/2}$ ionization energies (228.8 and 458.9, respectively), MoS_2 and TiO_2 are present.

Discussion

Characterization of MoS_2 Films on 52100 Steel Substrates. The goal of this investigation was to investigate the possibility of depositing MoS_2 films on steel substrates by AACVD for the use as a solid lubricant. This work builds upon that of previous studies, using $Mo(S_2CNEt_2)_4$ (**1**) as an AACVD precursor,[13] by characterizing the atmospheric thermal behavior of the precursor, as well as the morphology of the MoS_2 film when deposited onto 52100 steel substrates.

Because AACVD film growth occurs at atmospheric pressure, it is informative to first conduct thermal analysis that simulates more closely this process. The present analysis shows that complex **1** decomposes in three steps between 150 and 310 °C, losing ethylene and dithiocarbamate units, resulting in MoS_2 with minimal decomposed ligand contamination (Figure 1).

$MosS_2$ film growth studies at atmospheric pressure were conducted, and we determined that 400 °C was the optimum film growth temperature, affording growth rates of 16 nm/min. XRD and GXRD of films **A** grown on glass substrates confirmed an earlier report[13] of preferred orientation of weakly crystalline hexagonal phase MoS_2 (Figures 2 and 3A). The presence of MoS_2 was confirmed on films **B** grown on 52100 steel via XPS (Figure 4), whereas GXRD shows strong FeS reflections (Figure 3B). However, the Fe 2p ionization energies in the XPS spectrum are shifted to somewhat higher binding energies than that expected for Fe(II)-S (707 eV).[29] Having sputtered the film surface (∼35 nm), this observation cannot be attributed to surface oxidation. Thus, it is proposed that a relatively crystalline FeS layer is formed between the substrate and the MoS_2 film. The penetration depth for GXRD is on the order of 1−2 μm deep vs XPS, which penetrates only a few nanometers below the surface.[30] This is consistent with why FeS is observed in the former measurement, but not the latter.

SEM images of film **B** on 52100 steel reveal a different MoS_2 film morphology than that on glass substrates (Figure 5). From GXRD, there is some preferential orientation of FeS crystalline planes along the (00*l*) direction, meaning that there is preferred crystallite orientation with the basal planes parallel to the substrate surface. No reflections from MoS_2 are observed. From the SEM images, nanoparticles appear to grow as platelets perpendicular to the substrate surface. This is suggestive of type I MoS_2 films (terminology of Fleischauer[31]), where crystallite plane edges are predominately exposed. This would seem to result in a low surface area of the (001) crystalline planes, potentially meaning reduced lubricity. Tribological scratch evaluations were performed on film **B** to determine the coefficient of friction (μ; Figure 6). At room temperature, $\mu = 0.12$ and decreases to 0.10 as the substrate temperature reaches 100 °C, which is attributed to loss of water adsorbed on the surface of the films. It is possible that the FeS formed in the deposition of the films contributes to the lubrication, as it is known to be a good solid lubricant as well. Indeed, coefficients of friction below 0.2 for FeS have been reported.[32] However, it is doubtful that it is the sole reason for the tribology of the present films because burnishing (rubbing) of type I MoS_2 can act to partially orient the crystallites parallel to the substrate, thereby lubricating the surface.[31] As the substrate temperature is raised above 100 °C, μ increases above the room-temperature value. This increase is attributed to MoS_2 oxidation. This oxidation process to MoO_3 and H_2SO_4 is known to occur for MoS_2 and to increase the coefficient of friction at higher temperatures.[15] Indeed, XPS of the film **B** after high-temperature friction testing confirms the presence of MoO_3 and the absence of MoS_2.

(29) Mullet, M.; Boursiqot, S.; Abdelmoula, M.; Genin, J.-M.; Ehrhardt, J.-J. *Geochim. Cosmochim. Acta* **2002**, *66*, 829–836.
(30) (a) Debnath, S.; Predecki, P.; Suryanarayanan, R. *Pharm. Res.* **2004**, *21*, 149–159. (b) Rafaja, D. *Adv. Solid State Phys.* **2001**, *41*, 275–286. (c) Tilinin, I. S.; Jablonski, A.; Werner, W. S. M. *Prog. Surf. Sci.* **1996**, *52*, 25–40.
(31) (a) Fleischauer, P. D. *Thin Solid Films* **1987**, *154*, 309–322. (b) Fleischauer, P. D. *ASLE Trans.* **1983**, *27*, 82–88.
(32) Petersen, J. H.; Reitz, H.; Benzon, M. E.; Boetiger, J.; Chavallier, J.; Mikkelsen, N. J.; Morgen, P. *Surf. Coat. Technol.* **2004**, *179*, 165–175.

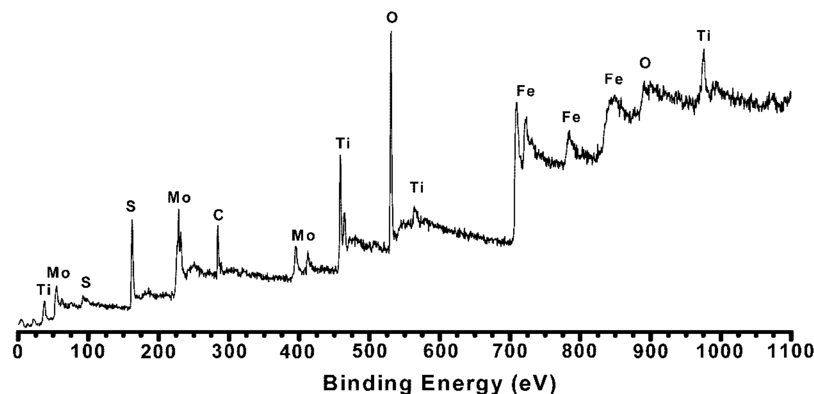

Figure 9. XPS spectrum of MoS_2 film **E** deposited on 52100 steel by AACVD using precursors **1** and **2**. Peaks are labeled with their corresponding element.

Incorporation of Ti in MoS_2 Films Using AACVD. This investigation was originally intended to employ $Ti(S^tBu)_4$ (**2**) to introduce Ti in conjunction with MoS_2 growth using complex **1** as a means of doping the MoS_2 films with Ti to enhance oxidative stability. Initial attempts to grow films by AACVD with toluene solutions of precursors **1** and **2** yielded only MoS_2 films, with negligible Ti content as determined by XPS and ICP. THF was then used as the solvent, and the Ti composition in the films as assayed by ICP/OES, varied from the **2**:**1** molar ratio contained in the precursor solution. Results are summarized in Table 1 for film **C**−**F** growth on glass and on 52100 steel substrates. As shown in Figure 7, reflections due to TiO_2 are detectible by GXRD in film **D**, with 89% Mo and 11% Ti as determined by ICP/OES. The presence of TiO_2 was unexpected, as the growth was conducted under Ar, and rigorous purification techniques were used to ensure dry, oxygen-free THF. Therefore, O sources must be from the ambient exposure after film growth or from possible reaction with THF during the AACVD process. XPS also confirms the presence of TiO_2, from the binding energy of the Ti $2p_{3/2}$ ionization peak, even after sputtering the film surface (Figure 9). This rules out oxidation of TiS_2 because of contact with air. A previous study reports that the decomposition of THF occurs on the surface of MoS_2 at temperatures above 150 °C.[33] Products from the decomposition include small hydrocarbons, aldehydes, and CO_2. The thiolate ligand complexed with Ti should be reactive to these species, whereas oxophilic Ti(IV) should readily coordinate to carbonyl and alkoxy compounds, ultimately leading to TiO_2.

As more TiO_2 is codeposited with MoS_2, the microstructural texture of the films changes, as seen in the SEM images (Figure 8). The ribbon-like network associated with the MoS_2 disappears, which is supported by the GXRD data (Figure 7), as the baseline pattern of the glass substrate becomes more pronounced, in concert with the diminished MoS_2 reflection intensities of the higher Ti-content films. XPS analysis of the films gives similar results to that of film **E**, revealing the presence of Mo $3d_{5/2}$ and S $2p_{3/2}$ ionization energies corresponding well with MoS_2, and the Ti $2p_{3/2}$ ionization energies corresponding to TiO_2. The Fe $2p_{3/2}$ energy position matches that of iron oxide, with no Fe(II)−S contribution detectible.

High-temperature scratch tests shows neglible improvement in lubrication performance with the Ti codeposition accompanying MoS_2 film growth.

Conclusions

Aerosol-assisted CVD has been used to deposit MoS_2 films using $Mo(S_2CNEt_2)_4$ (**1**) as the precursor onto 52100 steel substrates so that its tribological performance could be assessed. The morphology of the films consists of an initial crystalline layer of FeS, the subsequent growth of MoS_2 nanoparticles, the plane edges of which are predominately exposed perpendicular to the substrate surface. Low coefficients of friction arise from the combined performance of the FeS layer and burnishing of the MoS_2 nanoparticle films.

Titanium was incorporated into the MoS_2 films grown by AACVD using $Ti(S^tBu)_4$ as the titanium source. Codeposition of preferentially oriented TiO_2 appears to arise from the decomposition of the solvent (THF) on the MoS_2 nanoparticles and subsequent oxidation of the titanium precursor. Films grown on 52100 steel again exhibited the crystalline FeS layer forming between substrate and the MoS_2/TiO_2 films. No significant improvement in the tribological performance of the films was detected.

Acknowledgment. We thank the NSF (Grant CMS-0510895) for support of this research, and the Northwestern Materials Research Center (NSF MRSEC Grant DMR-0520513) for providing characterization facilities. We thank Dr. J. Carsello for assistance with X-ray diffraction measurements.

CM7026674

(33) Juzkow, M. W.; Gay, I. D. *J. Phys. Chem.* **1991**, *95*, 9911–9914.